Manuscript prepared for Atmos. Chem. Phys.
with version 2015/04/24 7.83 Copernicus papers of the LaTeX class copernicus.cls.
Date: 31 October 2016

First detection of ammonia (NH_3) in the Asian summer monsoon upper troposphere

Michael Höpfner[1], Rainer Volkamer[2,3], Udo Grabowski[1], Michel Grutter[4], Johannes Orphal[1], Gabriele Stiller[1], Thomas von Clarmann[1], and Gerald Wetzel[1]

[1]Institute of Meteorology and Climate Research, Karlsruhe Institute of Technology, Karlsruhe, Germany.
[2]Department of Chemistry & Biochemistry, University of Colorado, Boulder, CO, USA.
[3]Cooperative Institute for Research in Environmental Sciences, University of Colorado at Boulder, CO, USA.
[4]Centro de Ciencias de la Atmósfera, Universidad Nacional Autónoma de México, Mexico City, Mexico.

Correspondence to: M. Höpfner (michael.hoepfner@kit.edu)

Abstract. Ammonia (NH_3) has been detected in the upper troposphere by analysis of averaged MIPAS (Michelson Interferomter for Passive Atmospheric Sounding) infrared limb-emission spectra. We have found enhanced amounts of NH_3 within the region of the Asian summer monsoon at 12–15 km altitude. Three-monthly, 10° longitude × 10° latitude average profiles reaching maximum mixing ratios of around 30 $pptv$ in this altitude range have been retrieved with a vertical resolution of 3–8 km and estimated errors of about 5 $pptv$. These observations show that loss processes during transport from the boundary layer to the upper troposphere within the Asian monsoon do not deplete the air entirely of NH_3. Thus, ammonia might contribute to the so-called Asian tropopause aerosol layer by formation of ammonium aerosol particles. On a global scale, outside the monsoon area and during different seasons, we could not detect enhanced values of NH_3 above the actual detection limit of about 3-5 $pptv$. This upper bound helps to constrain global model simulations.

1 Introduction

In the Earth's atmosphere the trace gas ammonia (NH_3) represents the major form of reduced nitrogen. With a share of around 70–80%, the bulk of ammonia emissions is due to anthropogenic activity, namely the use of synthetic fertilizers and livestock manure management (Bouwman et al., 1997; Paulot et al., 2015). Major source regions of NH_3 are located in south-east China and northern India (Paulot et al., 2014; Van Damme et al., 2015).

Neutralization of acids by the alkaline gas NH_3 leads to the formation of ammonium salts in the atmosphere. For example, reaction of NH_3 with sulfuric acid (H_2SO_4) or nitric acid (HNO_3) forms aerosol particles composed of ammonium sulfate, $(NH_4)_2SO_4$, or ammonium nitrate, NH_4NO_3 (e.g. Behera et al., 2013, and references therein). These inorganic aerosols are important not only

with regard to air quality considerations (Hamaoui-Laguel et al., 2014) but they also affect climate through various direct and indirect radiative impacts (Adams et al., 2001; Martin et al., 2004; Liao and Seinfeld, 2005; Forster et al., 2007; Xu and Penner, 2012; Boucher et al., 2013). Further, cirrus clouds might also be affected by the presence of NH_3 and ammonium (Tabazadeh and Toon, 1998; Wang et al., 2008). E.g. ammonium sulfate aerosols that are partially coated and have exposed surface sites are active with respect to ice nucleation (Prenni et al., 2001; Wise et al., 2004). Such a heterogeneous nucleation pathway might influence size and number of cirrus particles and, consequently their radiative impact (Abbatt et al., 2006). Moreover, through stabilization of sulfuric acid clusters, ammonia itself may play an important role regarding the initial nucleation of sulfuric acid aerosols (Ortega et al., 2008; Kirkby et al., 2011; Schobesberger et al., 2013; Kürten et al., 2015).

Global emissions of NH_3 are expected to rise strongly due to the need to sustain a growing population and due to enhanced emissions under increasing temperatures (Erisman et al., 2008; Vuuren et al., 2011; Sutton et al., 2013). As a result, in future prospects for a positive radiative forcing by a decrease of the shortwave albedo caused by reductions of industrial SO_2 emissions may partly be compensated by increasing amounts of ammonium containing aerosols (Bellouin et al., 2011; Xu and Penner, 2012; Shindell et al., 2013; Hauglustaine et al., 2014).

With regard to the predicted increase in NH_3 emissions and the possible compensating effect on aerosol radiative forcing, Paulot et al. (2016) emphasize the need to better constrain also the vertical distribution of ammonia. However, there is very little information from measurements on NH_3 at mid- and upper tropospheric levels.

Before 2008, measurements of ammonia were almost exclusively based on in-situ technologies (von Bobrutzki et al., 2010). Compared to the wealth of observations on ground, vertical profiles of NH_3 from in-situ observations above the boundary layer are relatively sparse. Recently, aircraft-borne campaign measurements over the US obtained concentration profiles in the free troposphere reaching altitudes of about 6 km (Nowak et al., 2007; Nowak et al., 2010, 2012; Leen et al., 2013; Schiferl et al., 2016). At these altitudes maximum observed NH_3 mixing ratios reached about 800 pptv (Schiferl et al., 2016) with detection limits of 70 pptv (Nowak et al., 2010). In-situ air-borne observations over Germany by Ziereis and Arnold (1986) restricted concentrations to the sub-pptv range at altitudes between 8 and 10 km . To our knowledge, these are the only upper tropospheric in-situ-measurements of NH_3 published so far.

A first step in the direction of observations with global coverage was achieved by Beer et al. (2008), who reported the detection of NH_3 in the lower troposphere from space-borne nadir sounding measurements by the Tropospheric Emission Spectrometer (TES) on the EOS Aura satellite. Subsequently, various papers have been published describing retrieval, validation and interpretation of NH_3 derived from the nadir sounders TES (Clarisse et al., 2010; Shephard et al., 2011), IASI (Infrared Atmospheric Sounding Interferometer) (Coheur et al., 2009; Clarisse et al., 2009, 2010; Van Damme et al., 2014), CrIS (Cross-track Infrared Sounder) (Shephard and Cady-Pereira, 2015),

and AIRS (Atmospheric Infrared Sounder) (Warner et al., 2016). The vertical sensitivity of these satellite retrievals is mainly limited to the lower troposphere up to about 3–4 km and no altitude resolution is achieved (e.g., Clarisse et al., 2010; Shephard and Cady-Pereira, 2015). Recently, retrievals of NH_3 vertical column amounts from ground-based FTIR solar observations located at various sites have been presented by Dammers et al. (2015) and are being used for the quantitative validation of space-borne nadir-viewing datasets (Dammers et al., 2016). As shown by Dammers et al. (2015) in case of high amounts of NH_3 near the surface, the retrieval sensitivity peaks within the boundary layer where also the altitude-gradient can be derived. For low concentrations, the retrieval is only sensitive to the total vertical column amount.

To achieve vertically resolved profiles of trace gases in the upper troposphere and above, limb-sounding techniques have been applied frequently. Regarding ammonia, Oelhaf et al. (1983) reported upper limits of 100 pptv above 10 km by analysis of balloon-borne limb solar absorption spectra measured over the US. Space-borne solar occultation measurements obtained with the ACE-FTS instrument within a plume of biomass burning over Tanzania have been studied by Coheur et al. (2007). In that publication, the authors mention a "tentative identification" of NH_3 in the spectra, while the spectral signals of various other trace species, such as C_2H_4, C_3H_6O, H_2CO and PAN were detected unequivocally. Nonetheless, Coheur et al. (2007) derived a vertical profile of NH_3 between 6.5 and 17 km with typical values of less than 20 pptv and a maximum of about 50 pptv at 8 km. Burgess et al. (2006) report on first attempts to retrieve global distributions of ammonia using limb infrared emission spectra measured by the Michelson Interferometer for Passive Atmospheric Sounding (MIPAS) on Envisat. They obtained one climatological vertical profile with NH_3 volume mixing ratios below 5 pptv at altitudes above 9 km. However, no evidence for the presence of NH_3 in the limb spectra nor any indication for enhanced values within the area of the Asian summer monsoon is shown.

In summary, considering the reported observations, neither the in-situ measurements by Ziereis and Arnold (1986) nor the limb-sounding remote sensing data (Oelhaf et al., 1983; Coheur et al., 2007; Burgess et al., 2006) prove the presence of ammonia at altitudes above about 8 km. In the work presented below we show, to our knowledge, the first evidence for NH_3 together with quantitative retrievals at upper tropospheric levels by use of MIPAS averaged limb spectra.

2 MIPAS/Envisat

On board the Envisat satellite the MIPAS limb sounder recorded infrared spectra of the radiation emitted by atmospheric constituents from June 2002 until April 2012 (Fischer et al., 2008). Between June 2002 and March 2004 (period 1), the spectral resolution was 0.025 cm^{-1} with one limb-scan consisting of 17 spectra from about 6–60 km altitude with steps of 3 km up to about 42 km in the case of nominal mode observations. From January 2005 until April 2012 (period 2), the spectral

resolution was degraded to 0.0625 cm^{-1}. This was accompanied by a better vertical sampling (27 tangent levels up to about 70 km altitude with 1.5 km steps up to ≈23 km). Also in the horizontal direction along the satellite track the sampling improved from a distance between subsequent limb-scans of 550 km during period 1 to 420 km during period 2.

3 Retrieval and spectral detection

Here we report on the detection and retrieval of $\mathrm{NH_3}$ from MIPAS observations in the upper troposphere on the basis of averaged limb-spectra. This method has already been applied successfully for the detection of bromine nitrate ($\mathrm{BrONO_2}$) (Höpfner et al., 2009) and for the compilation of a global climatology of stratospheric sulfur dioxide ($\mathrm{SO_2}$) from MIPAS measurements (Höpfner et al., 2013). In those investigations the mean spectra consisted of monthly zonal averages within 10° latitude intervals, whereas for the present work we have chosen seasonal (3-monthly) averages within bins of 10° latitude by 10° longitude. Thus, we have refrained from zonal averaging in order to obtain resolution in the meridional direction, albeit slightly sacrificing temporal resolution. To reduce the spectral noise by at least a factor of five, we have chosen a lower limit of 25 single spectra (MIPAS level-1b version 5) for averaging. The resulting mean number of co-added spectra per time/latitude/longitude bin varies from 53–56 for the years 2003 and 2007 to 65–70 for 2008–2011 reaching maximum numbers of around 140 (see supplemental material for the detailed geographical and temporal distribution). This leads to a typical reduction of the spectral noise by 0.1 ranging from 0.2 to 0.08 and signal-to-noise values resulting in retrieval errors near and below 1 pptv of $\mathrm{NH_3}$ (see detailed error estimation below). In the troposphere the number of available spectra is limited as a result of cloud contamination along the limb line-of-sight. We have applied a cloud filter to deselect cloud-contaminated spectra before averaging. For the cloud detection scheme the established cloud-index method (Spang et al., 2004) with a cloud index limit of 2.0 has been used.

To derive altitude profiles of $\mathrm{NH_3}$ from each averaged limb-scan we have applied a constrained non-linear multi-parameter least-squares fitting procedure whereby measurements from all spectra of one limb scan are analysed in one step (e.g., von Clarmann et al., 2003; Höpfner et al., 2009). The unknown atmospheric state is described in terms of trace gas volume mixing ratios at discrete altitude levels with a grid distance of 1 km. This grid is finer compared to the instrumental vertical field-of-view width of about 3 km at the tangent points and also finer than the vertical sampling distance of 1.5–3 km. To dampen vertical oscillations arising from the ill-posedness of the inverse problem a first order smoothing constraint has been chosen (Tikhonov, 1963; Steck, 2002). The regularization strengths have been adjusted independently for each species being retrieved simultaneously.

For fitting of the $\mathrm{NH_3}$ signatures we have chosen spectral windows within the interval 950–970 cm^{-1}, which have the advantage that they are situated in the region of one of the optically thinnest mid-infrared atmospheric windows. Furthermore, there are relatively few spectrally inter-

fering species which have to be retrieved simultaneously with NH_3. Spectroscopic line parameters of the HITRAN 2012 database (Rothman et al., 2013) have been used.

A scheme consisting of two steps has been identified as adequate for the retrieval of NH_3. First, the broader wavenumber range 962–968 cm^{-1} has been chosen to fit the strong CO_2 lines of the laser band together with the interfering species O_3, H_2O, NH_3, COF_2. In the second step, narrow analysis windows have been placed around the strongest signatures of NH_3: 951.6–952.0 cm^{-1}, 965.1–965.6 cm^{-1}, and 966.6–967.5 cm^{-1} (MIPAS period 1) and 951.625–952.0 cm^{-1}, 965.125–965.625 cm^{-1}, and 966.625–967.5 cm^{-1} (MIPAS period 2), thereby avoiding the peaks of the strong CO_2 lines. At this stage CO_2 is kept fixed to the results from the initial retrieval, while O_3, H_2O and COF_2 are retrieved jointly with NH_3.

Figure 1 presents the spectral fit and the detection of NH_3 for examples from both MIPAS periods at tangent heights around 12.5 km within the region of the Asian monsoon in June-August 2003 (top panel) and 2009 (bottom panel). Within each panel the top row shows the observations in black, the fit without taking NH_3 into account in blue and the retrieval including NH_3 in red. In the second row of each panel the residual spectra are shown for the retrieval without (blue) and with (red) consideration of NH_3. Here the green line is the difference between the two simulations (with minus without NH_3) in order to show the spectral signature of NH_3 without any instrumental effect, such as spectral noise.

The top panel of Fig. 1 reveals clearly the presence of NH_3 in MIPAS limb spectra. Radiative transfer simulations without consideration of NH_3 lead to largest residuals (bold blue curves) at the position of the ammonia lines (dotted orange curves). Only when ammonia is taken into account are the observed spectra within all three microwindows fitted sufficiently well. Comparing the first row of the bottom panel in Fig. 1 with that of the top panel, the worse spectral resolution of MIPAS period 2 becomes obvious. Still the residuals of the NH_3 spectral lines and the better fit upon their consideration are visible, especially in microwindows 2 and 3.

Results of the altitude dependent error estimation are presented in Fig. 2 for the two examples of the limb scans for which the spectral fits have been shown in Fig. 1. A summary of the assumptions on the various sources of uncertainty is provided in Table 1. For spectral noise, the actual error numbers referring to the two limb-scans discussed are given together with their range over all observations in brackets. While noise is directly mapped into the state space for each individual retrieval, the error estimation for all other uncertainties has been performed by sensitivity calculations for atmospheric conditions representative for observations within the influence of the Asian monsoon (Höpfner et al., 2009; Höpfner et al., 2013).

In the left panels of Fig. 2 the bold dotted curves indicate the reconstructed vertical profiles of NH_3. The concentrations reach maximum values of around 24–29 $pptv$. The bold solid lines represent the total error calculated as the square root of the sum of all squared error components. The total errors amount to around 2–6 $pptv$ (17–80%, right panels) in the altitude region up to about

20 km. Above, the estimated errors are larger than the mixing ratios of NH_3. The leading error components are tangent altitude uncertainties, uncertainties in the HITRAN line intensity data of NH_3 and nonlinearity effects in the averaging procedure as discussed in Höpfner et al. (2009). On the other hand, the use of averaged spectra reduces the noise term to less than 1 pptv within the altitude range of interest.

The vertical resolution of the resulting altitude profiles of NH_3 mixing ratios is directly connected to the noise error values through the applied setting of the regularization strength. The altitude resolution of the retrieval is described by the retrieval averaging kernel matrix (Rodgers, 2000). Examples for both MIPAS periods are provided in Fig. 3. From these, typical vertical resolutions are derived as the retrieval grid width divided by the inverse of the diagonal matrix elements (Rodgers, 2000). The globally average vertical resolution at the altitude levels 12, 15, and 18 km, which are discussed in more detail below, is 6.6 km, 7.9 km and 8.8 km during period 1 and 3.5 km, 4.3 km, and 5.6 km during period 2.

4 The global dataset

Retrievals of NH_3 have been performed for the entire period of MIPAS observations, i.e. from July 2002 until April 2012. Figure 4 presents the global volume mixing ratio distributions at 15 km altitude during seven seasons from July 2002 until February 2004. There are enhanced values of up to 33 pptv within a region between 30°–110°E and 20°–50°N during boreal summer, coinciding with the occurrence of the Asian monsoons. During all other seasons of the two MIPAS periods and outside the region influenced by the Asian monsoon, no similarly high concentrations of NH_3 can be found within the entire altitude region covered by our measurements.

An overview for all years with sufficient data coverage in the Asian summer monsoon season during the MIPAS mission lifetime is provided in Fig. 5 for altitude levels of 12, 15, and 18 km. Due to the less frequent presence of clouds, the number of pixels with valid measurements increases with altitude. Similar to the results from MIPAS period 1, also during period 2 the enhancement of NH_3 within the Asian monsoon region is present for all years of observation. Further, on a global scale there are no other areas visible in the dataset with similarly enhanced values of NH_3. While at 12 and 15 km altitude NH_3 enhancements compared to the global background state are visible during all years, at 18 km altitude increased values of NH_3 are present only during the years 2003, 2008, and 2010.

A comparison between vertical profiles of NH_3 averaged within the western (30–70°E, solid lines) and eastern (70–110°E, dashed lines) parts of the monsoon region for the latitude band 30–40°N is presented in Fig. 6 for the years 2003 and 2007–2011. In the same Figure, the dotted curves show the NH_3 mean Jun/Jul/Aug profiles for all years outside the Asian monsoon area, for the same longitude and latitude range (30–110°E, 30–40°S) of the southern hemisphere. The profiles in the region of

the Asian monsoon reveal that the maximum concentrations over the whole altitude range within one year are always larger in the eastern part of the Asian monsoon compared to the western part. Maximum concentrations of NH_3 in the eastern part reach about 10–22 pptv at 11-13 km altitude. Largest values are found in 2003 and 2009 and lowest ones in 2007 and 2011.

In the western part of the area influenced by the Asian monsoon, enhanced averaged volume mixing ratios of NH_3 can be observed during the years 2003, 2008, and 2010 with values ranging from 6 to 15 pptv. Situated at around 13–15 km, the maximum concentrations in the western part are always located at higher altitudes compared to those from the eastern part of the monsoon region. The position of the NH_3 maximum at higher altitudes in the western compared to the eastern part of the monsoon system might be due to convective uplift of boundary layer air in the east followed by upper tropospheric transport and further uplift towards the west. Such an uplift of air from east to west is indicated in Vogel et al. (2014, Fig. 10) by trajectory calculations, however mainly located at the border of the anticyclone.

The mean NH_3 profiles of the western part show no clear enhancements during the years 2007, 2009 and 2011. These profiles exhibit maximum values below 5 pptv, which are in the range of concentrations retrieved in the case of the 'background' state of the southern hemisphere (indicated by dotted lines in Fig. 6). These values are below our estimated detection limit (see below).

Due to the lack of ammonia observations in the upper troposphere, we cannot validate our dataset with correlative measurements. However, in the next section we discuss its plausibility by comparing with the few previous observations and atmospheric model results.

5 Discussion

As mentioned in the introduction, observations of NH_3 reaching upper tropospheric levels have been published by Ziereis and Arnold (1986). They report upper limits of about 0.04 pptv between 8 and 10 km over Germany in May 1985. At the present state of our MIPAS data analysis we cannot contradict those upper values outside the influence of the Asian summer monsoon system. Given the total error of a few pptv we would estimate the 1-σ detection limit of our retrieval to be about 3–5 pptv. One might argue that the use of a 1-σ detection limit does not provide sufficiently significant evidence of the NH_3 enhancement within the monsoon. However, random errors cannot explain why the enhancements should appear in a contiguous geographical pattern nor could they account for the enhancements appearing only in one season.

For example within the data shown in Fig. 5 at 12 km, there are 176 values larger than 5 pptv outside the region 20–50°N $\times$ 30-120°E compared to 55 inside. However, at the 15 km level, only 5 data points exceed 5 pptv outside but 37 inside. Using 2-σ, there are no data points outside compared to 23 and 15 exceeding 10 pptv inside the region at 12 km and 15 km, respectively. Further, the detected enhancements inside the monsoon region are in many cases (13 times at 12 km and 8 times

at 15 km) even above 15 pptv and, thus, larger than a 3-σ limit. Temporally resolved, values above 10 pptv in the monsoon region exist during all years at both altitude levels with the exception of 2011 at 15 km. 15 pptv are exceeded at 10 km in 2003–2010 and at 15 km in all years but 2007 and 2011.

Regarding the retrievals outside the monsoon area, there is a difference between the two MIPAS measurement periods at 10–12 km altitude (see e.g. the difference in the dotted lines in Fig. 6 or the higher background level at 12 km altitude visible in Fig. 5 between the year 2003 and 2007–2011) that reaches 4 pptv. We attribute this discrepancy to an unexplained systematic uncertainty caused by the different spectral resolutions between the two instrumental states. This observation corroborates our error estimation and supports our conclusion that retrieved values up to 3–5 pptv are below the detection limit of the actual dataset.

Nonetheless, our measurements impose constraints on the global distribution of upper tropospheric NH_3 concentrations which can be compared to results from model calculations. One of the first globally modeled distributions of NH_3 was presented by Dentener and Crutzen (1994, their Fig. 2b). These calculations were based on the tropospheric transport model Moguntia with a horizontal resolution of $10^\circ \times 10^\circ$with 10 layers up to 100 hPa in combination with, at that time, the first global emission inventory of NH_3 with the same resolution as the transport model. Yearly mean mixing ratios of below 2 pptv are modeled at upper tropospheric levels at mid- and high-latitudes. These are consistent with the MIPAS background values. However, at equatorial and sub-tropical latitudes, annual mean values of some tens of pptv were simulated between 300 hPa (≈9.5 km) and 200 hPa (≈12.5 km) which are clearly larger than the MIPAS results. Dentener and Crutzen (1994) attributed these values to natural emissions in the tropics. The comparison with our results indicates that either these emissions might have been overestimated or the tropical sink processes of NH_3 underestimated. In their conclusions Dentener and Crutzen (1994) also mention high modeled concentrations of NH_3 in the free troposphere over India and China. However, since these enhancements were not quantified, they cannot be compared to our observations.

In contrast to the results of Dentener and Crutzen (1994), the zonal and yearly averages of modeled NH_3 shown in Feng and Penner (2007, Fig. 9) decrease to well below 10 pptv above 500 hPa (≈6 km) also in tropical regions. Their aerosol chemistry transport model (Umich/IMPACT) had a horizontal resolution of 2° latitude × 2.5° longitude with 26 layers up to 0.1 hPa using the $1^\circ \times 1^\circ$global NH_3 emission inventory of Bouwman et al. (1997). Thus, these global model results are more compatible with the MIPAS dataset.

Globally resolved annual mean model results of NH_3 are given in Adams et al. (1999, Plate 3a). These data were based on runs with the general circulation model GISS GCM II-prime with 4° latitude × 5° longitude horizontal resolution, nine vertical layers up to 10 hPa and NH_3 emissions according to Bouwman et al. (1997). Mean mixing ratios of about 3.2 pptv at the 200 hPa pressure level (≈12.5/11 km in tropical/polar regions) are reported. At that pressure level, a slight gradient

between the two hemispheres is visible, with values of 0–1 pptv in the south and 3–10 pptv in the north. We do not recognize such a gradient in the background $\mathrm{NH_3}$ concentrations from the MIPAS measurements, although, given our estimated error, we cannot conclusively refute such a gradient.

Regarding ammonium nitrate aerosol during the Asian monsoon season, Metzger et al. (2002) discuss their model results of enhanced values at upper tropospheric levels over Asia. They used the global chemistry-transport model TM3 with 7.5° latitude × 10° longitude horizontal resolution, 19 vertical levels and the EDGAR database for the emissions of $\mathrm{NH_3}$. These high amounts of ammonium nitrate over Asia are attributed to in-situ production from $\mathrm{NH_3}$ (and $\mathrm{HNO_3}$) being convectively transported to upper tropospheric levels. The fact that $\mathrm{NH_3}$ is not removed by dissolution in droplets and subsequent rainout is explained by the low acidity of convective clouds, such that only part of the $\mathrm{NH_3}$ would be dissolved. Our observations support these results with respect to the enhanced amounts of $\mathrm{NH_3}$ which obviously survive the uplift within the Asian monsoon circulation. This indicates that a part of the Asian tropopause aerosol layer (ATAL) (Vernier et al., 2011) might be composed of ammonium nitrate, ammonium sulfate or other ammonium containing particles.

Further, through a possible influence of the Asian monsoon on the composition of the tropical tropopause layer (TTL) by transport of ammonia or ammonium, our measurements may help to explain why in-situ measurements of aerosols in the TTL indicate that the sulfate appears to be mostly or fully neutralized (Froyd et al., 2009, 2010). Measurements of particle acidity hold potential to inform low $\mathrm{NH_3}$ concentrations further in the background UT outside the Asian summer monsoon system.

6 Conclusions

We have presented first evidence of ammonia being present in the Earth's upper troposphere above $10\ \mathrm{km}$ by analysis of MIPAS infrared limb emission spectra. The region and period of detection is confined to the Asian summer monsoon system. Maximum average values of around 30 pptv over a three-month period have been retrieved, thus demonstrating that part of the $\mathrm{NH_3}$ released at the ground survives the loss processes on its way to the upper troposphere. As suggested by Metzger et al. (2002), ammonia may form ammonium nitrate aerosols under those circumstances. Thus, our observations indicate a possible contribution of ammonium aerosols to the composition of the ATAL.

The detection of enhanced amounts of $\mathrm{NH_3}$ in the western part of the Asian monsoon anticyclone during several years suggests that its lifetime is long enough to survive transport to areas far from the source region. The generally lower mixing ratios of $\mathrm{NH_3}$ in the western compared to the eastern part indicate ongoing loss processes at high altitudes.

Unfortunately, in the literature there seem to exist no locally resolved model results of $\mathrm{NH_3}$ during the monsoon period to which we could compare our observations. We anticipate that such simulations would be of value to improve our understanding of $\mathrm{NH_3}$ loss processes and aerosol production

in the Asian monsoon. Also, airborne remote sensing observations, like the one planned within the EU project StratoClim with the GLORIA instrument on the Geophysica high flying aircraft, would strongly increase our knowledge about ammonia distributions in the Asian monsoon on a much finer time, horizontal and vertical resolution scale than the MIPAS dataset presented here.

Regarding the global distribution of upper tropospheric NH_3 outside the Asian monsoon, within this study we could provide upper limits in the range of a few pptv. This will help to constrain global models and to improve their results.

The NH_3 dataset is available upon request from the author or at http://www.imk-asf.kit.edu/english/308.php.

Acknowledgements. We thank Michelle Santee, a second reviewer and the editor Rolf Müller for their constructive comments and Bärbel Vogel for helpful discussions. Provision of MIPAS level-1b calibrated spectra by ESA and meteorological analysis data by ECMWF is acknowledged. The research leading to these results has received funding from the European Community's Seventh Framework Programme (FP7/2007-2013) under grant agreement 603557. R.V. is recipient of a KIT Distinguished Intl Scholar award, and acknowledges funding from the U.S. National Science Foundation EAGER award AGS-1452317. We acknowledge support by the Deutsche Forschungsgemeinschaft and Open Access Publishing Fund of the Karlsruhe Institute of Technology.

References

Abbatt, J. P. D., Benz, S., Cziczo, D. J., Kanji, Z., Lohmann, U., and Möhler, O.: Solid Ammonium Sulfate Aerosols as Ice Nuclei: A Pathway for Cirrus Cloud Formation, Science, doi:10.1126/science.1129726, http://science.sciencemag.org/content/early/2006/08/31/science.1129726, 2006.

Adams, P. J., Seinfeld, J. H., and Koch, D. M.: Global concentrations of tropospheric sulfate, nitrate, and ammonium aerosol simulated in a general circulation model, J. Geophys. Res., 104, 13 791–13 823, doi:10.1029/1999JD900083, http://dx.doi.org/10.1029/1999JD900083, 1999.

Adams, P. J., Seinfeld, J. H., Koch, D., Mickley, L., and Jacob, D.: General circulation model assessment of direct radiative forcing by the sulfate-nitrate-ammonium-water inorganic aerosol system, J. Geophys. Res., 106, 1097–1111, doi:10.1029/2000JD900512, http://dx.doi.org/10.1029/2000JD900512, 2001.

Beer, R., Shephard, M. W., Kulawik, S. S., Clough, S. A., Eldering, A., Bowman, K. W., Sander, S. P., Fisher, B. M., Payne, V. H., Luo, M., Osterman, G. B., and Worden, J. R.: First satellite observations of lower tropospheric ammonia and methanol, Geophys. Res. Lett., 35, n/a–n/a, doi:10.1029/2008GL033642, http://dx.doi.org/10.1029/2008GL033642, 2008.

Behera, S. N., Sharma, M., Aneja, V. P., and Balasubramanian, R.: Ammonia in the atmosphere: a review on emission sources, atmospheric chemistry and deposition on terrestrial bodies, Environmental Science and Pollution Research, 20, 8092–8131, doi:10.1007/s11356-013-2051-9, http://dx.doi.org/10.1007/s11356-013-2051-9, 2013.

Bellouin, N., Rae, J., Jones, A., Johnson, C., Haywood, J., and Boucher, O.: Aerosol forcing in the Climate Model Intercomparison Project (CMIP5) simulations by HadGEM2-ES and the role of ammonium nitrate, J. Geophys. Res., 116, n/a–n/a, doi:10.1029/2011JD016074, http://dx.doi.org/10.1029/2011JD016074, d20206, 2011.

Boucher, O., Randall, D., Artaxo, P., Bretherton, C., Feingold, G., Forster, P., Kerminen, V.-M., Kondo, Y., Liao, H., Lohmann, U., Rasch, P., Satheesh, S., Sherwood, S., Stevens, B., and Zhang, X.: Clouds and Aerosols, Cambridge University Press, Cambridge, United Kingdom and New York, NY, USA, 2013.

Bouwman, A., Lee, D., Asman, W., Dentener, F., Van Der Hoek, K., and Olivier, J.: A global high-resolution emission inventory for ammonia, Global biogeochemical cycles, 11, 561–587, 1997.

Burgess, A., Dudhia, A., Grainger, R., and Stevenson, D.: Progress in tropospheric ammonia retrieval from the {MIPAS} satellite instrument, Adv. Space Res., 37, 2218 – 2221, doi:http://dx.doi.org/10.1016/j.asr.2005.06.073, http://www.sciencedirect.com/science/article/pii/S0273117705008367, 2006.

Clarisse, L., Clerbaux, C., Dentener, F., Hurtmans, D., and Coheur, P.-F.: Global ammonia distribution derived from infrared satellite observations, Nature Geosci., 2, 479–483, doi:10.1038/ngeo551, http://dx.doi.org/10.1038/ngeo551, 2009.

Clarisse, L., Shephard, M. W., Dentener, F., Hurtmans, D., Cady-Pereira, K., Karagulian, F., Van Damme, M., Clerbaux, C., and Coheur, P.-F.: Satellite monitoring of ammonia: A case study of the San Joaquin Valley, J. Geophys. Res., 115, n/a–n/a, doi:10.1029/2009JD013291, http://dx.doi.org/10.1029/2009JD013291, d13302, 2010.

Coheur, P.-F., Herbin, H., Clerbaux, C., Hurtmans, D., Wespes, C., Carleer, M., Turquety, S., Rinsland, C. P., Remedios, J., Hauglustaine, D., Boone, C. D., and Bernath, P. F.: ACE-FTS observation of a young biomass

burning plume: first reported measurements of C_2H_4, C_3H_6O, H_2CO and PAN by infrared occultation from space, Atmos. Chem. Phys., 7, 5437–5446, doi:10.5194/acp-7-5437-2007, http://www.atmos-chem-phys.net/7/5437/2007/, 2007.

Coheur, P.-F., Clarisse, L., Turquety, S., Hurtmans, D., and Clerbaux, C.: IASI measurements of reactive trace species in biomass burning plumes, Atmos. Chem. Phys., 9, 5655–5667, doi:10.5194/acp-9-5655-2009, http://www.atmos-chem-phys.net/9/5655/2009/, 2009.

Dammers, E., Vigouroux, C., Palm, M., Mahieu, E., Warneke, T., Smale, D., Langerock, B., Franco, B., Van Damme, M., Schaap, M., Notholt, J., and Erisman, J. W.: Retrieval of ammonia from ground-based FTIR solar spectra, Atmos. Chem. Phys., 15, 12 789–12 803, doi:10.5194/acp-15-12789-2015, http://www.atmos-chem-phys.net/15/12789/2015/, 2015.

Dammers, E., Palm, M., Van Damme, M., Vigouroux, C., Smale, D., Conway, S., Toon, G. C., Jones, N., Nussbaumer, E., Warneke, T., Petri, C., Clarisse, L., Clerbaux, C., Hermans, C., Lutsch, E., Strong, K., Hannigan, J. W., Nakajima, H., Morino, I., Herrera, B., Stremme, W., Grutter, M., Schaap, M., Wichink Kruit, R. J., Notholt, J., Coheur, P.-F., and Erisman, J. W.: An evaluation of IASI-NH_3 with ground-based Fourier transform infrared spectroscopy measurements, Atmos. Chem. Phys., 16, 10 351–10 368, doi:10.5194/acp-16-10351-2016, http://www.atmos-chem-phys.net/16/10351/2016/, 2016.

Dee, D. P., Uppala, S. M., Simmons, A. J., Berrisford, P., Poli, P., Kobayashi, S., Andrae, U., Balmaseda, M. A., Balsamo, G., Bauer, P., Bechtold, P., Beljaars, A. C. M., van de Berg, L., Bidlot, J., Bormann, N., Delsol, C., Dragani, R., Fuentes, M., Geer, A. J., Haimberger, L., Healy, S. B., Hersbach, H., Hólm, E. V., Isaksen, L., Kållberg, P., Köhler, M., Matricardi, M., McNally, A. P., Monge-Sanz, B. M., Morcrette, J.-J., Park, B.-K., Peubey, C., de Rosnay, P., Tavolato, C., Thépaut, J.-N., and Vitart, F.: The ERA-Interim reanalysis: configuration and performance of the data assimilation system, qjrms, 137, 553–597, doi:10.1002/qj.828, http://dx.doi.org/10.1002/qj.828, 2011.

Dentener, F. J. and Crutzen, P. J.: A three-dimensional model of the global ammonia cycle, Journal of Atmospheric Chemistry, 19, 331–369, doi:10.1007/BF00694492, http://dx.doi.org/10.1007/BF00694492, 1994.

Erisman, J. W., Sutton, M. A., Galloway, J., Klimont, Z., and Winiwarter, W.: How a century of ammonia synthesis changed the world, Nature Geosci., 1, 636–639, doi:10.1038/ngeo325, 2008.

Feng, Y. and Penner, J. E.: Global modeling of nitrate and ammonium: Interaction of aerosols and tropospheric chemistry, J. Geophys. Res., 112, n/a–n/a, doi:10.1029/2005JD006404, http://dx.doi.org/10.1029/2005JD006404, d01304, 2007.

Fischer, H., Birk, M., Blom, C., Carli, B., Carlotti, M., von Clarmann, T., Delbouille, L., Dudhia, A., Ehhalt, D., Endemann, M., Flaud, J. M., Gessner, R., Kleinert, A., Koopman, R., Langen, J., López-Puertas, M., Mosner, P., Nett, H., Oelhaf, H., Perron, G., Remedios, J., Ridolfi, M., Stiller, G., and Zander, R.: MIPAS: an instrument for atmospheric and climate research, Atmos. Chem. Phys., 8, 2151–2188, 2008.

Forster, P., Ramaswamy, V., Artaxo, P., Berntsen, T., Betts, R., Fahey, D., Haywood, J., Lean, J., Lowe, D., Myhre, G., Nganga, J., Prinn, R., Raga, G., Schulz, M., and Van Dorland, R.: Changes in Atmospheric Constituents and in Radiative Forcing, pp. 129–243, Cambridge University Press, Cambridge, United Kingdom and New York, NY, USA, 2007.

Froyd, K. D., Murphy, D. M., Sanford, T. J., Thomson, D. S., Wilson, J. C., Pfister, L., and Lait, L.: Aerosol composition of the tropical upper troposphere, Atmospheric Chemistry and Physics, 9, 4363–4385, doi:10.5194/acp-9-4363-2009, http://www.atmos-chem-phys.net/9/4363/2009/, 2009.

Froyd, K. D., Murphy, D. M., Lawson, P., Baumgardner, D., and Herman, R. L.: Aerosols that form subvisible cirrus at the tropical tropopause, Atmospheric Chemistry and Physics, 10, 209–218, doi:10.5194/acp-10-209-2010, http://www.atmos-chem-phys.net/10/209/2010/, 2010.

Hamaoui-Laguel, L., Meleux, F., Beekmann, M., Bessagnet, B., Génermont, S., Cellier, P., and Létinois, L.: Improving ammonia emissions in air quality modelling for France, Atmospheric Environment, 92, 584 – 595, doi:http://dx.doi.org/10.1016/j.atmosenv.2012.08.002, http://www.sciencedirect.com/science/article/pii/S1352231012007662, 2014.

Hauglustaine, D. A., Balkanski, Y., and Schulz, M.: A global model simulation of present and future nitrate aerosols and their direct radiative forcing of climate, Atmos. Chem. Phys., 14, 11 031–11 063, doi:10.5194/acp-14-11031-2014, http://www.atmos-chem-phys.net/14/11031/2014/, 2014.

Höpfner, M., von Clarmann, T., Fischer, H., Funke, B., Glatthor, N., Grabowski, U., Kellmann, S., Kiefer, M., Linden, A., Milz, M., Steck, T., Stiller, G. P., Bernath, P., Blom, C. E., Blumenstock, T., Boone, C., Chance, K., Coffey, M. T., Friedl-Vallon, F., Griffith, D., Hannigan, J. W., Hase, F., Jones, N., Jucks, K. W., Keim, C., Kleinert, A., Kouker, W., Liu, G. Y., Mahieu, E., Mellqvist, J., Mikuteit, S., Notholt, J., Oelhaf, H., Piesch, C., Reddmann, T., Ruhnke, R., Schneider, M., Strandberg, A., Toon, G., Walker, K. A., Warneke, T., Wetzel, H., Wood, S., and Zander, R.: Validation of MIPAS $ClONO_2$ measurements, Atmos. Chem. Phys., 7, 257–281, 2007.

Höpfner, M., Orphal, J., von Clarmann, T., Stiller, G., and Fischer, H.: Stratospheric $BrONO_2$ observed by MIPAS, Atmos. Chem. Phys., 9, 1735–1746, 2009.

Höpfner, M., Glatthor, N., Grabowski, U., Kellmann, S., Kiefer, M., Linden, A., Orphal, J., Stiller, G., von Clarmann, T., Funke, B., and Boone, C. D.: Sulfur dioxide (SO_2) as observed by MIPAS/Envisat: temporal development and spatial distribution at 15–45 km altitude, Atmos. Chem. Phys., 13, 10 405–10 423, doi:10.5194/acp-13-10405-2013, http://www.atmos-chem-phys.net/13/10405/2013/, 2013.

Kiefer, M., von Clarmann, T., Grabowski, U., De Laurentis, M., Mantovani, R., Milz, M., and Ridolfi, M.: Characterization of MIPAS elevation pointing, Atmos. Chem. Phys., 7, 1615–1628, 2007.

Kirkby, J., Curtius, J., Almeida, J., Dunne, E., Duplissy, J., Ehrhart, S., Franchin, A., Gagné, S., Ickes, L., Kürten, A., Kupc, A., Metzger, A., Riccobono, F., Rondo, L., Schobesberger, S., Tsagkogeorgas, G., Wimmer, D., Amorim, A., Bianchi, F., Breitenlechner, M., David, A., Dommen, J., Downard, A., Ehn, M., Flagan, R. C., Haider, S., Hansel, A., Hauser, D., Jud, W., Junninen, H., Kreissl, F., Kvashin, A., Laaksonen, A., Lehtipalo, K., Lima, J., Lovejoy, E. R., Makhmutov, V., Mathot, S., Mikkilä, J., Minginette, P., Mogo, S., Nieminen, T., Onnela, A., Pereira, P., Petäjä, T., Schnitzhofer, R., Seinfeld, J. H., Sipilä, M., Stozhkov, Y., Stratmann, F., Tomé, A., Vanhanen, J., Viisanen, Y., Vrtala, A., Wagner, P. E., Walther, H., Weingartner, E., Wex, H., Winkler, P. M., Carslaw, K. S., Worsnop, D. R., Baltensperger, U., and Kulmala, M.: Role of sulphuric acid, ammonia and galactic cosmic rays in atmospheric aerosol nucleation, Nature, 476, 429–433, doi:10.1038/nature10343, 2011.

Kleinert, A., Aubertin, G., Perron, G., Birk, M., Wagner, G., Hase, F., Nett, H., and Poulin, R.: MIPAS Level 1B algorithms overview: operational processing and characterization, Atmos. Chem. Phys., 7, 1395–1406, doi:10.5194/acp-7-1395-2007, http://www.atmos-chem-phys.net/7/1395/2007/, 2007.

Kürten, A., Münch, S., Rondo, L., Bianchi, F., Duplissy, J., Jokinen, T., Junninen, H., Sarnela, N., Schobesberger, S., Simon, M., Sipilä, M., Almeida, J., Amorim, A., Dommen, J., Donahue, N. M., Dunne, E. M., Flagan, R. C., Franchin, A., Kirkby, J., Kupc, A., Makhmutov, V., Petäjä, T., Praplan, A. P., Riccobono, F., Steiner, G., Tomé, A., Tsagkogeorgas, G., Wagner, P. E., Wimmer, D., Baltensperger, U., Kulmala, M., Worsnop, D. R., and Curtius, J.: Thermodynamics of the formation of sulfuric acid dimers in the binary (H_2SO_4–H_2O) and ternary (H_2SO_4–H_2O–NH_3) system, Atmos. Chem. Phys., 15, 10 701–10 721, doi:10.5194/acp-15-10701-2015, http://www.atmos-chem-phys.net/15/10701/2015/, 2015.

Leen, J. B., Yu, X.-Y., Gupta, M., Baer, D. S., Hubbe, J. M., Kluzek, C. D., Tomlinson, J. M., and Mike R. Hubbell, I.: Fast In Situ Airborne Measurement of Ammonia Using a Mid-Infrared Off-Axis ICOS Spectrometer, Environmental Science & Technology, 47, 10 446–10 453, doi:10.1021/es401134u, http://dx.doi.org/10.1021/es401134u, pMID: 23869496, 2013.

Liao, H. and Seinfeld, J. H.: Global impacts of gas-phase chemistry-aerosol interactions on direct radiative forcing by anthropogenic aerosols and ozone, J. Geophys. Res., 110, n/a–n/a, doi:10.1029/2005JD005907, http://dx.doi.org/10.1029/2005JD005907, d18208, 2005.

Martin, S. T., Hung, H.-M., Park, R. J., Jacob, D. J., Spurr, R. J. D., Chance, K. V., and Chin, M.: Effects of the physical state of tropospheric ammonium-sulfate-nitrate particles on global aerosol direct radiative forcing, Atmos. Chem. Phys., 4, 183–214, doi:10.5194/acp-4-183-2004, http://www.atmos-chem-phys.net/4/183/2004/, 2004.

Metzger, S., Dentener, F., Krol, M., Jeuken, A., and Lelieveld, J.: Gas/aerosol partitioning 2. Global modeling results, J. Geophys. Res., 107, ACH 17–1–ACH 17–23, doi:10.1029/2001JD001103, http://dx.doi.org/10.1029/2001JD001103, 2002.

Nowak, J. B., Neuman, J. A., Kozai, K., Huey, L. G., Tanner, D. J., Holloway, J. S., Ryerson, T. B., Frost, G. J., McKeen, S. A., and Fehsenfeld, F. C.: A chemical ionization mass spectrometry technique for airborne measurements of ammonia, J. Geophys. Res., 112, D10S02, doi:10.1029/2006JD007589, 2007.

Nowak, J. B., Neuman, J. A., Bahreini, R., Brock, C. A., Middlebrook, A. M., Wollny, A. G., Holloway, J. S., Peischl, J., Ryerson, T. B., and Fehsenfeld, F. C.: Airborne observations of ammonia and ammonium nitrate formation over Houston, Texas, J. Geophys. Res., 115, n/a–n/a, doi:10.1029/2010JD014195, http://dx.doi.org/10.1029/2010JD014195, d22304, 2010.

Nowak, J. B., Neuman, J. A., Bahreini, R., Middlebrook, A. M., Holloway, J. S., McKeen, S. A., Parrish, D. D., Ryerson, T. B., and Trainer, M.: Ammonia sources in the California South Coast Air Basin and their impact on ammonium nitrate formation, Geophys. Res. Lett., 39, n/a–n/a, doi:10.1029/2012GL051197, http://dx.doi.org/10.1029/2012GL051197, l07804, 2012.

Oelhaf, H., Leupolt, A., and Fischer, H.: Discrepancies between balloon-borne IR atmospheric spectra and corresponding synthetic spectra calculated line by line around 825 cm^{-1}, Appl. Opt., 22, 647–649, 1983.

Ortega, I. K., Kurtén, T., Vehkamäki, H., and Kulmala, M.: The role of ammonia in sulfuric acid ion induced nucleation, Atmos. Chem. Phys., 8, 2859–2867, doi:10.5194/acp-8-2859-2008, http://www.atmos-chem-phys.net/8/2859/2008/, 2008.

Paulot, F., Jacob, D. J., Pinder, R. W., Bash, J. O., Travis, K., and Henze, D. K.: Ammonia emissions in the United States, European Union, and China derived by high-resolution inversion of ammonium wet deposition data: Interpretation with a new agricultural emissions inventory (MASAGE_NH3), J. Geophys. Res., 119, 4343–4364, doi:10.1002/2013JD021130, http://dx.doi.org/10.1002/2013JD021130, 2014.

Paulot, F., Jacob, D. J., Johnson, M. T., Bell, T. G., Baker, A. R., Keene, W. C., Lima, I. D., Doney, S. C., and Stock, C. A.: Global oceanic emission of ammonia: Constraints from seawater and atmospheric observations, Global Biogeochem. Cycles, 29, 1165–1178, doi:10.1002/2015GB005106, http://dx.doi.org/10.1002/2015GB005106, 2015GB005106, 2015.

Paulot, F., Ginoux, P., Cooke, W. F., Donner, L. J., Fan, S., Lin, M.-Y., Mao, J., Naik, V., and Horowitz, L. W.: Sensitivity of nitrate aerosols to ammonia emissions and to nitrate chemistry: implications for present and future nitrate optical depth, Atmos. Chem. Phys., 16, 1459–1477, doi:10.5194/acp-16-1459-2016, http://www.atmos-chem-phys.net/16/1459/2016/, 2016.

Ploeger, F., Gottschling, C., Griessbach, S., Grooß, J.-U., Guenther, G., Konopka, P., Müller, R., Riese, M., Stroh, F., Tao, M., Ungermann, J., Vogel, B., and von Hobe, M.: A potential vorticity-based determination of the transport barrier in the Asian summer monsoon anticyclone, Atmospheric Chemistry and Physics, 15, 13 145–13 159, doi:10.5194/acp-15-13145-2015, http://www.atmos-chem-phys.net/15/13145/2015/, 2015.

Prenni, A. J., Wise, M. E., Brooks, S. D., and Tolbert, M. A.: Ice nucleation in sulfuric acid and ammonium sulfate particles, Journal of Geophysical Research: Atmospheres, 106, 3037–3044, doi:10.1029/2000JD900454, http://dx.doi.org/10.1029/2000JD900454, 2001.

Rodgers, C. D.: Inverse Methods for Atmospheric Sounding: Theory and Practice, vol. 2 of *Series on Atmospheric, Oceanic and Planetary Physics*, World Scientific, 2000.

Rothman, L., Gordon, I., Babikov, Y., Barbe, A., Benner, D. C., Bernath, P., Birk, M., Bizzocchi, L., Boudon, V., Brown, L., Campargue, A., Chance, K., Cohen, E., Coudert, L., Devi, V., Drouin, B., Fayt, A., Flaud, J.-M., Gamache, R., Harrison, J., Hartmann, J.-M., Hill, C., Hodges, J., Jacquemart, D., Jolly, A., Lamouroux, J., Roy, R. L., Li, G., Long, D., Lyulin, O., Mackie, C., Massie, S., Mikhailenko, S., Müller, H., Naumenko, O., Nikitin, A., Orphal, J., Perevalov, V., Perrin, A., Polovtseva, E., Richard, C., Smith, M., Starikova, E., Sung, K., Tashkun, S., Tennyson, J., Toon, G., Tyuterev, V., and Wagner, G.: The {HITRAN2012} molecular spectroscopic database, J. Quant. Spectrosc. Radiat. Transfer, 130, 4 – 50, doi:http://dx.doi.org/10.1016/j.jqsrt.2013.07.002, http://www.sciencedirect.com/science/article/pii/S0022407313002859, {HITRAN2012} special issue, 2013.

Schiferl, L. D., Heald, C. L., Van Damme, M., Clarisse, L., Clerbaux, C., Coheur, P.-F., Nowak, J. B., Neuman, J. A., Herndon, S. C., Roscioli, J. R., and Eilerman, S. J.: Interannual variability of ammonia concentrations over the United States: sources and implications, Atmos. Chem. Phys., 16, 12 305–12 328, doi:10.5194/acp-16-12305-2016, http://www.atmos-chem-phys.net/16/12305/2016/, 2016.

Schobesberger, S., Junninen, H., Bianchi, F., Lönn, G., Ehn, M., Lehtipalo, K., Dommen, J., Ehrhart, S., Ortega, I. K., Franchin, A., Nieminen, T., Riccobono, F., Hutterli, M., Duplissy, J., Almeida, J., Amorim, A., Breitenlechner, M., Downard, A. J., Dunne, E. M., Flagan, R. C., Kajos, M., Keskinen, H., Kirkby, J., Kupc, A., Kürten, A., Kurtén, T., Laaksonen, A., Mathot, S., Onnela, A., Praplan, A. P., Rondo, L., Santos, F. D., Schallhart, S., Schnitzhofer, R., Sipilä, M., Tomé, A., Tsagkogeorgas, G., Vehkamäki, H., Wimmer, D., Baltensperger, U., Carslaw, K. S., Curtius, J., Hansel, A., Petäjä, T., Kulmala, M., Don-

ahue, N. M., and Worsnop, D. R.: Molecular understanding of atmospheric particle formation from sulfuric acid and large oxidized organic molecules, PNAS, 110, 17 223–17 228, doi:10.1073/pnas.1306973110, http://www.pnas.org/content/110/43/17223.abstract, 2013.

Shephard, M. W. and Cady-Pereira, K. E.: Cross-track Infrared Sounder (CrIS) satellite observations of tropospheric ammonia, Atmos. Meas. Techn., 8, 1323–1336, doi:10.5194/amt-8-1323-2015, http://www.atmos-meas-tech.net/8/1323/2015/, 2015.

Shephard, M. W., Cady-Pereira, K. E., Luo, M., Henze, D. K., Pinder, R. W., Walker, J. T., Rinsland, C. P., Bash, J. O., Zhu, L., Payne, V. H., and Clarisse, L.: TES ammonia retrieval strategy and global observations of the spatial and seasonal variability of ammonia, Atmos. Chem. Phys., 11, 10 743–10 763, doi:10.5194/acp-11-10743-2011, http://www.atmos-chem-phys.net/11/10743/2011/, 2011.

Shindell, D. T., Lamarque, J.-F., Schulz, M., Flanner, M., Jiao, C., Chin, M., Young, P. J., Lee, Y. H., Rotstayn, L., Mahowald, N., Milly, G., Faluvegi, G., Balkanski, Y., Collins, W. J., Conley, A. J., Dalsoren, S., Easter, R., Ghan, S., Horowitz, L., Liu, X., Myhre, G., Nagashima, T., Naik, V., Rumbold, S. T., Skeie, R., Sudo, K., Szopa, S., Takemura, T., Voulgarakis, A., Yoon, J.-H., and Lo, F.: Radiative forcing in the ACCMIP historical and future climate simulations, Atmos. Chem. Phys., 13, 2939–2974, doi:10.5194/acp-13-2939-2013, http://www.atmos-chem-phys.net/13/2939/2013/, 2013.

Spang, R., Remedios, J. J., and Barkley, M. P.: Colour indices for the detection and differentiation of cloud types in infra-red limb emission spectra, Adv. Space Res., 33, 1041–1047, 2004.

Steck, T.: Methods for determining regularization for atmospheric retrieval problems, Appl. Opt., 41, 1788–1797, 2002.

Sutton, M. A., Reis, S., Riddick, S. N., Dragosits, U., Nemitz, E., Theobald, M. R., Tang, Y. S., Braban, C. F., Vieno, M., Dore, A. J., Mitchell, R. F., Wanless, S., Daunt, F., Fowler, D., Blackall, T. D., Milford, C., Flechard, C. R., Loubet, B., Massad, R., Cellier, P., Personne, E., Coheur, P. F., Clarisse, L., Van Damme, M., Ngadi, Y., Clerbaux, C., Skjøth, C. A., Geels, C., Hertel, O., Wichink Kruit, R. J., Pinder, R. W., Bash, J. O., Walker, J. T., Simpson, D., Horváth, L., Misselbrook, T. H., Bleeker, A., Dentener, F., and de Vries, W.: Towards a climate-dependent paradigm of ammonia emission and deposition, Philosophical Transactions of the Royal Society of London B: Biological Sciences, 368, doi:10.1098/rstb.2013.0166, http://rstb.royalsocietypublishing.org/content/368/1621/20130166, 2013.

Tabazadeh, A. and Toon, O. B.: The role of ammoniated aerosols in cirrus cloud nucleation, Geophys. Res. Lett., 25, 1379–1382, doi:10.1029/97GL03585, http://dx.doi.org/10.1029/97GL03585, 1998.

Tikhonov, A.: On the solution of incorrectly stated problems and method of regularization, Dokl. Akad. Nauk. SSSR, 151, 501–504, 1963.

Van Damme, M., Clarisse, L., Heald, C. L., Hurtmans, D., Ngadi, Y., Clerbaux, C., Dolman, A. J., Erisman, J. W., and Coheur, P. F.: Global distributions, time series and error characterization of atmospheric ammonia (NH_3) from IASI satellite observations, Atmos. Chem. Phys., 14, 2905–2922, doi:10.5194/acp-14-2905-2014, http://www.atmos-chem-phys.net/14/2905/2014/, 2014.

Van Damme, M., Erisman, J. W., Clarisse, L., Dammers, E., Whitburn, S., Clerbaux, C., Dolman, A. J., and Coheur, P.-F.: Worldwide spatiotemporal atmospheric ammonia (NH3) columns variability revealed by satellite, Geophys. Res. Lett., 42, 8660–8668, doi:10.1002/2015GL065496, http://dx.doi.org/10.1002/2015GL065496, 2015GL065496, 2015.

Vernier, J.-P., Thomason, L. W., and Kar, J.: CALIPSO detection of an Asian tropopause aerosol layer, Geophys. Res. Lett., 38, doi:10.1029/2010GL046614, http://dx.doi.org/10.1029/2010GL046614, 2011.

Vogel, B., Günther, G., Müller, R., Grooß, J.-U., Hoor, P., Krämer, M., Müller, S., Zahn, A., and Riese, M.: Fast transport from Southeast Asia boundary layer sources to northern Europe: rapid uplift in typhoons and eastward eddy shedding of the Asian monsoon anticyclone, Atmos. Chem. Phys., 14, 12 745–12 762, doi:10.5194/acp-14-12745-2014, http://www.atmos-chem-phys.net/14/12745/2014/, 2014.

von Bobrutzki, K., Braban, C. F., Famulari, D., Jones, S. K., Blackall, T., Smith, T. E. L., Blom, M., Coe, H., Gallagher, M., Ghalaieny, M., McGillen, M. R., Percival, C. J., Whitehead, J. D., Ellis, R., Murphy, J., Mohacsi, A., Pogany, A., Junninen, H., Rantanen, S., Sutton, M. A., and Nemitz, E.: Field inter-comparison of eleven atmospheric ammonia measurement techniques, Atmos. Meas. Techn., 3, 91–112, doi:10.5194/amt-3-91-2010, http://www.atmos-meas-tech.net/3/91/2010/, 2010.

von Clarmann, T., Glatthor, N., Grabowski, U., Höpfner, M., Kellmann, S., Kiefer, M., Linden, A., Mengistu Tsidu, G., Milz, M., Steck, T., Stiller, G. P., Wang, D. Y., Fischer, H., Funke, B., Gil-López, S., and López-Puertas, M.: Retrieval of temperature and tangent altitude pointing from limb emission spectra recorded from space by the Michelson Interferometer for Passive Atmospheric Sounding (MIPAS), J. Geophys. Res., 108, 4736, doi:10.1029/2003JD003602, 2003.

von Clarmann, T., Höpfner, M., Kellmann, S., Linden, A., Chauhan, S., Funke, B., Grabowski, U., Glatthor, N., Kiefer, M., Schieferdecker, T., Stiller, G. P., and Versick, S.: Retrieval of temperature, H_2O, O_3, HNO_3, CH_4, N_2O, $ClONO_2$ and ClO from MIPAS reduced resolution nominal mode limb emission measurements, Atmos. Meas. Techn., 2, 159–175, 2009.

Vuuren, D. P., Edmonds, J., Kainuma, M., Riahi, K., Thomson, A., Hibbard, K., Hurtt, G. C., Kram, T., Krey, V., Lamarque, J.-F., Masui, T., Meinshausen, M., Nakicenovic, N., Smith, S. J., and Rose, S. K.: The representative concentration pathways: an overview, Climatic Change, 109, 5–31, doi:10.1007/s10584-011-0148-z, http://dx.doi.org/10.1007/s10584-011-0148-z, 2011.

Wang, J., Hoffmann, A. A., Park, R. J., Jacob, D. J., and Martin, S. T.: Global distribution of solid and aqueous sulfate aerosols: Effect of the hysteresis of particle phase transitions, J. Geophys. Res., 113, n/a–n/a, doi:10.1029/2007JD009367, http://dx.doi.org/10.1029/2007JD009367, d11206, 2008.

Warner, J. X., Wei, Z., Strow, L. L., Dickerson, R. R., and Nowak, J. B.: The global tropospheric ammonia distribution as seen in the 13-year AIRS measurement record, Atmospheric Chemistry and Physics, 16, 5467–5479, doi:10.5194/acp-16-5467-2016, http://www.atmos-chem-phys.net/16/5467/2016/, 2016.

Wise, M. E., Garland, R. M., and Tolbert, M. A.: Ice nucleation in internally mixed ammonium sulfate/dicarboxylic acid particles, Journal of Geophysical Research: Atmospheres, 109, n/a–n/a, doi:10.1029/2003JD004313, http://dx.doi.org/10.1029/2003JD004313, d19203, 2004.

Xu, L. and Penner, J. E.: Global simulations of nitrate and ammonium aerosols and their radiative effects, Atmos. Chem. Phys., 12, 9479–9504, doi:10.5194/acp-12-9479-2012, http://www.atmos-chem-phys.net/12/9479/2012/, 2012.

Ziereis, H. and Arnold, F.: Gaseous ammonia and ammonium ions in the free troposphere, Nature, 321, 503–505, doi:10.1038/321503a0, 1986.

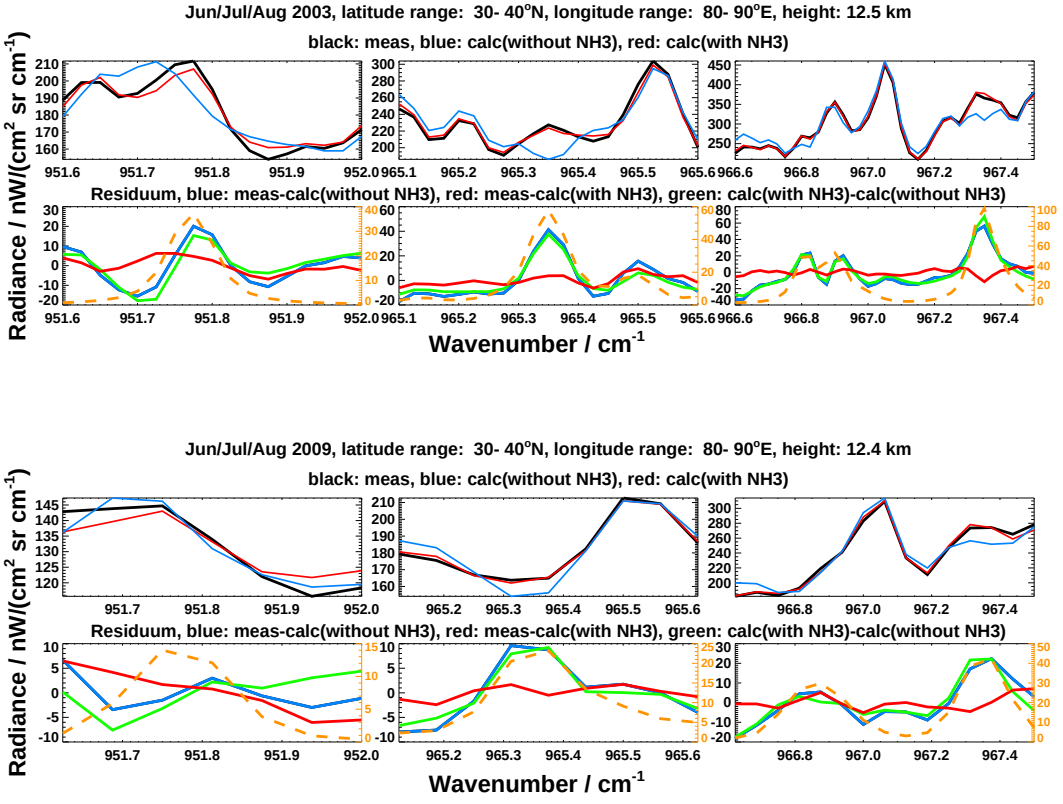

Figure 1. Spectral identification of NH_3 in MIPAS observations within the three spectral windows used for the retrieval (columns). The top two rows belong to the first observational period with higher spectral resolution. Rows 3 and 4 refer to the second period with lower spectral resolution. Rows 1 and 3 contain measured (black) and best fit spectra (blue: without, red: with NH_3). Row 2 and 4 show the spectral residuals without consideration of NH_3 (blue) and with NH_3 (red). Green curves in the second and fourth row represent the spectral features of NH_3 (calculation with NH_3 minus calculation without NH_3). To guide the eye, the orange dashed lines in rows 2 and 4 are simulated pure NH_3 spectra.

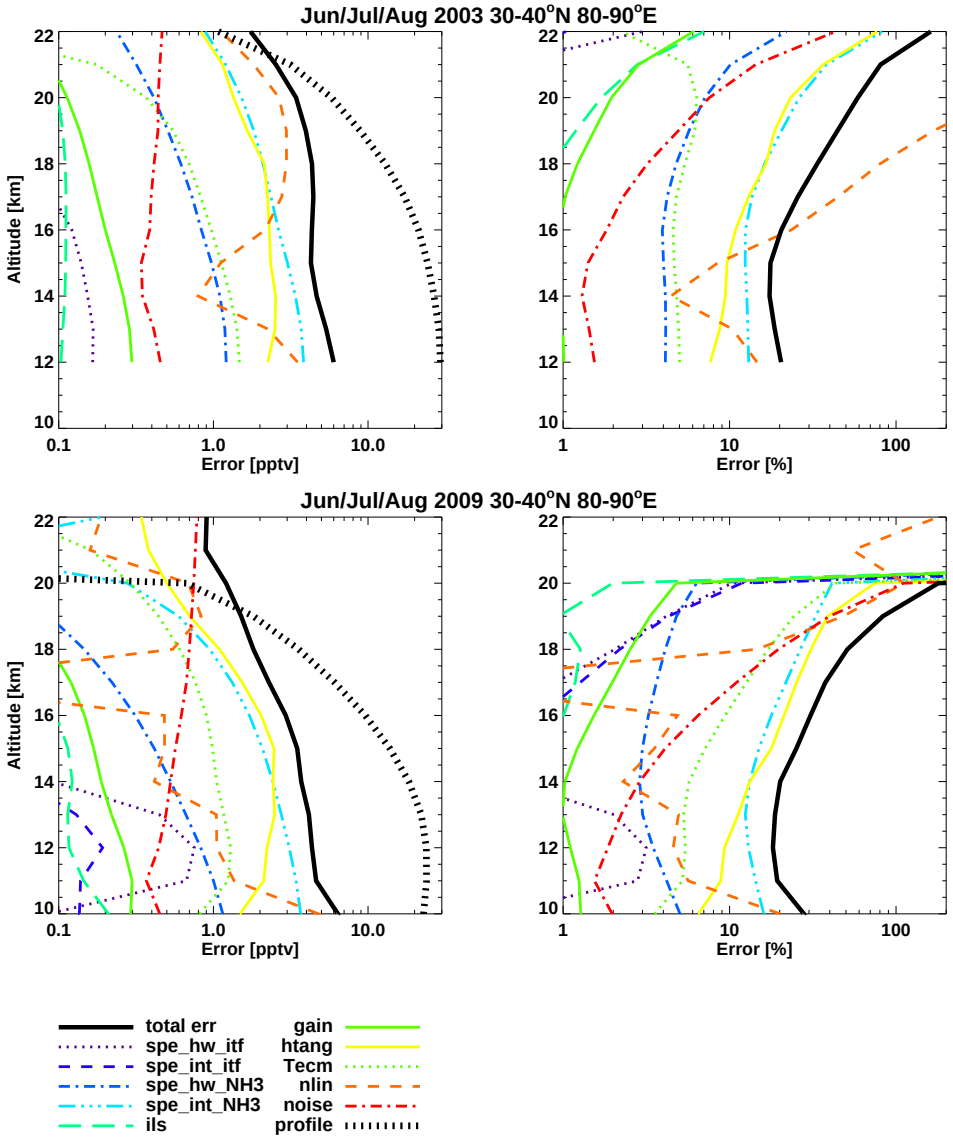

Figure 2. Estimated error profiles for two examples: one from measurement period 1 (June/July/August 2003, 30–40°N, 80–90°E) and one from period 2 (June/July/August 2009, 30–40°N, 80–90°E). The retrieved NH_3 profiles are shown as bold black dotted lines ("profile"). Abbreviations of the error sources are resolved in Tab. 1.

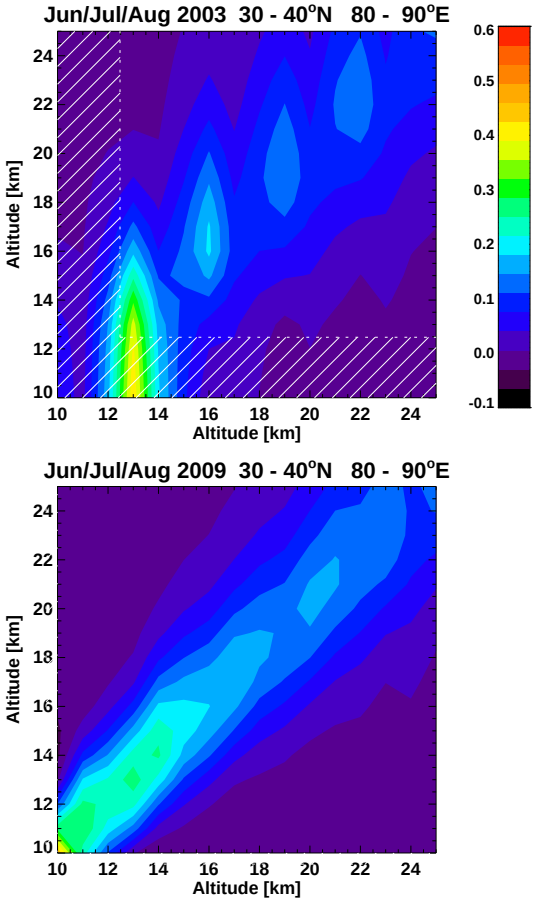

Figure 3. Averaging kernels of the MIPAS NH_3 retrieval during the first (top) and second (bottom) MIPAS measurement period. The number of degrees-of-freedom up to 25 km is 2.1 (top) and 3.5 (bottom). Hatched areas indicate altitudes below the lowest tangent height where no measurement information is available.

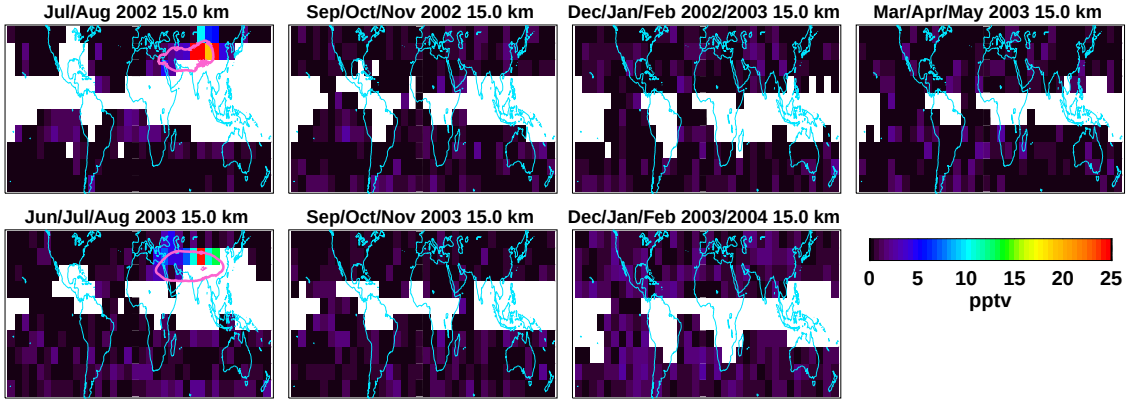

Figure 4. Distributions of NH_3 volume mixing ratios at 15 km altitude between 50°N and 50°S retrieved from MIPAS seasonal mean spectra during the first measurement period. Pixels where not enough spectra for averaging were available are left white. To guide the eye, the pink lines denote the approximate position of the Asian Monsoon Anticyclone. It is the 2×10^{-6} $\mathrm{Km^2kg^{-1}s^{-1}}$ contour of the mean potential vorticity for July/August in 2002 and June/July/August in 2003 at the potential temperature level of 370 K from the ECMWF ERA interim reanalysis (Dee et al., 2011) (e.g. Ploeger et al., 2015, and references therein).

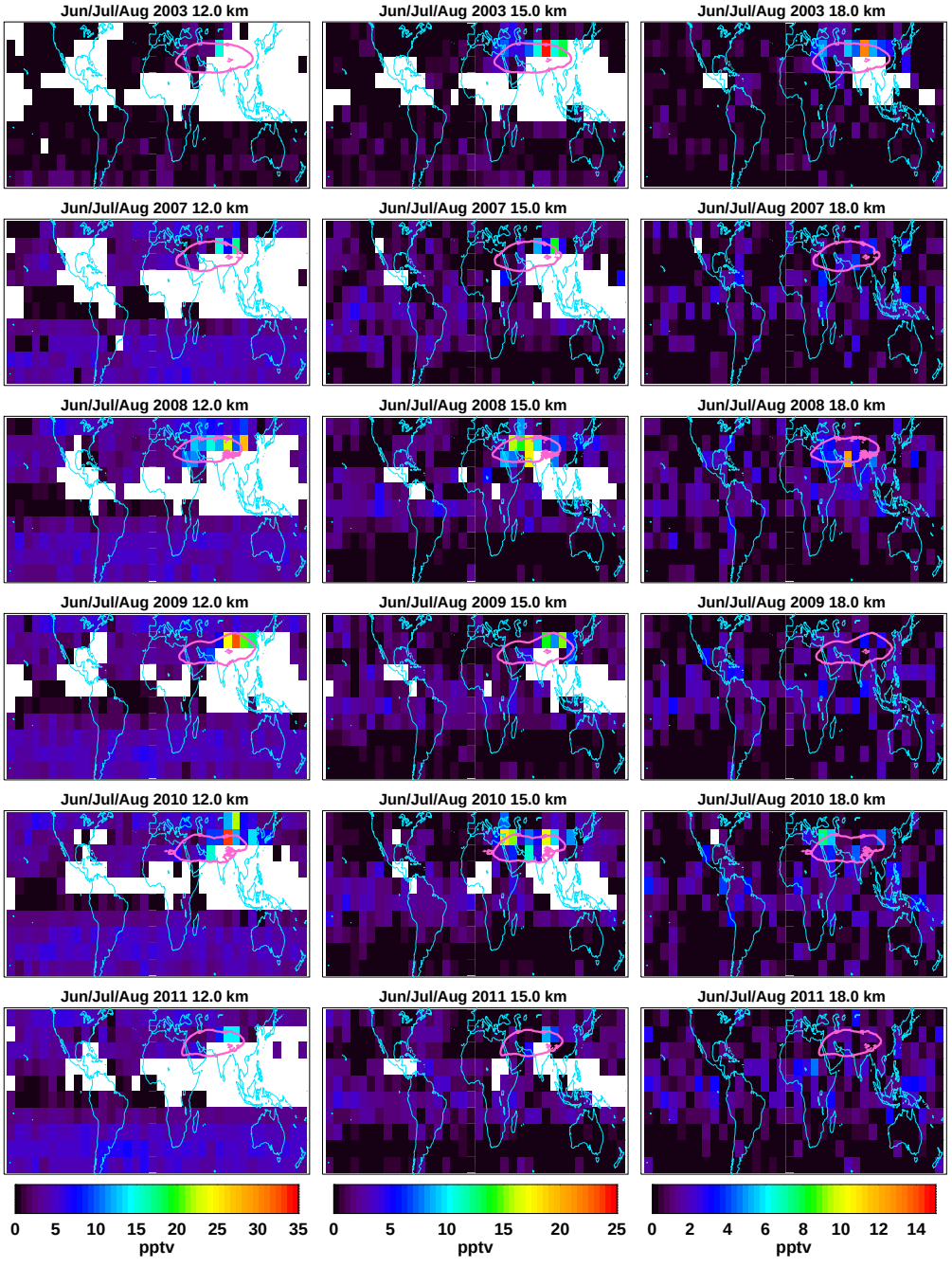

Figure 5. Distributions of NH_3 volume mixing ratios at 12 km, 15 km and 18 km altitude between 50°N and 50°S retrieved from MIPAS seasonal mean spectra during the Asian monsoon period for several years. Pixels where not enough spectra for averaging were available are left white. Pink contour lines denote the mean position of the Asian Monsoon Anticyclone for June/July/August as described in the caption of Fig. 4.

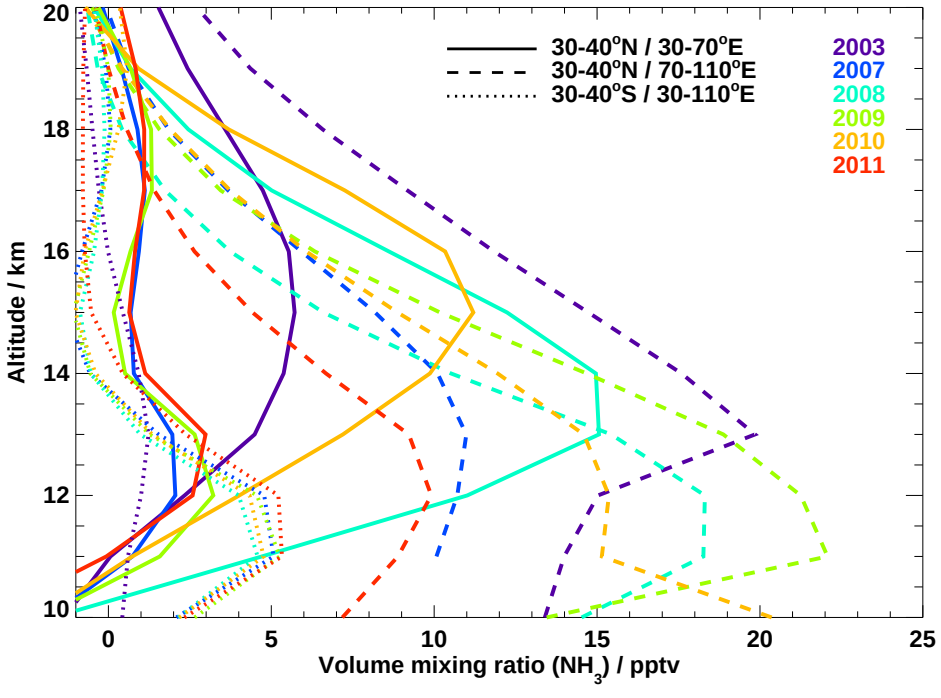

Figure 6. Mean profiles of NH_3 from MIPAS within the geographical range noted in the figure legend during June/July/August of each year. Solid: western part, dashed: eastern part of the Asian monsoon, dotted: reference profiles outside the monsoon in the southern hemisphere.

Table 1. Assumptions on uncertainties used for the error assessment in Fig. 2.

Error source	Assumed uncertainty	Abbreviation
Spectral noise after apodization[1]	period 1: 2.2 (1.5–3.1) $\mathrm{nW/(cm^2 sr\,cm^{-1})}$	noise
	period 2: 1.3 (0.8–1.8) $\mathrm{nW/(cm^2 sr\,cm^{-1})}$	
Instrument line shape[2]	3%	ils
Instrument gain calibration[3]	1%	gain
Tangent altitude[4]	300 m	htang
Temperature[5]	2 K below/5 K above 35 km	Tecm
Retrieval from averaged spectra[6]		nlin
Air-broadened half-width of NH_3 lines[7]	10%	spe_hw_NH_3
Intensity of NH_3 lines[7]	15%	spe_int_NH_3
Air-broadened half-width of interfering gas lines[7]	15%	spe_hw_itf
Intensity of interfering gas lines[7]	5%	spe_int_itf

[1] ESA l1b dataset, depending on number of co-added spectra; [2] F. Hase, pers. comm., Höpfner et al. (2007); [3] Kleinert et al. (2007); [4] von Clarmann et al. (2003); von Clarmann et al. (2009); Kiefer et al. (2007); [5] ECMWF uncertainty Höpfner et al. (2013); [6] Höpfner et al. (2009); Höpfner et al. (2013); [7] HITRAN 2012 spectral line errors Rothman et al. (2013)